

A 23 m.y. record of low atmospheric CO₂

Ying Cui¹, Brian A. Schubert^{2*} and A. Hope Jahren³¹Department of Earth and Environmental Studies, Montclair State University, Montclair, New Jersey 07043, USA²School of Geosciences, University of Louisiana at Lafayette, Lafayette, Louisiana 70504, USA³Centre for Earth Evolution and Dynamics, University of Oslo, N-0315 Oslo, Norway

ABSTRACT

Current atmospheric CO₂ concentration is known to be higher than it has been during the past ~800 k.y. of Earth history, based on direct measurement of CO₂ within ice cores. A comparison to the more ancient past is complicated by a deficit of CO₂ proxies that may be applied across very long spans of geologic time. Here, we present a new CO₂ record across the past 23 m.y. of Earth history based on the δ¹³C value of terrestrial C₃ plant remains, using a method applicable to the entire ~400 m.y. history of C₃ photosynthesis on land. Across the past 23 m.y., CO₂ likely ranged between ~230 ppmv and 350 ppmv (68% confidence interval: ~170–540 ppm). CO₂ was found to be highest during the early and middle Miocene and likely below present-day levels during the middle Pliocene (84th percentile: ~400 ppmv). These data suggest present-day CO₂ (412 ppmv) exceeds the highest levels that Earth experienced at least since the Miocene, further highlighting the present-day disruption of long-established CO₂ trends within Earth's atmosphere.

INTRODUCTION

Knowledge of atmospheric CO₂ concentration is vital for understanding Earth's climate system because it imparts a controlling effect on global temperatures across recent (Hegerl et al., 2006) and geologic (Foster et al., 2017) time scales. Proxies (Breecker et al., 2010) and models (Royer et al., 2014) indicate that CO₂ has varied widely during the geologic past. Direct measurement of CO₂ has been performed at the Mauna Loa Observatory (Hawaii, USA) for the past 60+ yr, and historical CO₂ has been sampled continuously from ice-core bubbles recording the past 800 k.y. (Petit et al., 1999; Lüthi et al., 2008), allowing for trends in CO₂ during the latter portion of the Quaternary to be evaluated in detail. Direct observations of atmospheric greenhouse gases are also now available from discontinuous ice up to 2 m.y. old from East Antarctica (Higgins et al., 2015; Yan et al., 2019).

For time periods older than the Pleistocene, many CO₂ proxies have been applied, including the proportion of epidermal cells that are stomatal pores (Kürschner et al., 1996, 2008; Beerling et al., 2009; Grein et al., 2013; Wang et al., 2015; Reichgelt et al., 2016); the stable carbon isotope composition of paleosol carbonate (Breecker

and Cerling, 1992; Ekart et al., 1999; Retallack, 2014; Da et al., 2015, 2019); alkenones derived from marine phytoplankton (Seki et al., 2010; Badger et al., 2013a, 2013b; Zhang et al., 2013); and the pH of ocean water as derived from boron isotopes (Bartoli et al., 2011; Foster et al., 2012; Greenop et al., 2014; Martinez-Boti et al., 2015; Stap et al., 2016). Each of these proxies provides robust results for specific time periods (Foster et al., 2017; Hollis et al., 2019); however, a CO₂ proxy for use across the entire history of vascular land plants (i.e., the past ~400 m.y.) is lacking.

Here, we present a method for calculating CO₂ that is based on a ubiquitous substrate, is sensitive across a wide range of CO₂, and is rooted in a fully understood mechanism of response to changing CO₂. We illustrate its efficacy by presenting a novel, high-resolution record of CO₂ for the Neogene through the Quaternary (i.e., the past 23 m.y.), a period that lacks a continuous record of CO₂ from any single proxy.

Our approach is centered upon the δ¹³C value of C₃ vascular land plants (hereafter δ¹³C_p), which is available from terrestrial sediments for most of the Phanerozoic (Nordt et al., 2016). Our calculations of CO₂ assumed that global changes in atmospheric composition affect the plant tissues of all terrestrial C₃ plants via the

universally shared mechanism of photorespiration. Because CO₂ is well mixed in Earth's atmosphere, and diminished photorespiration with increasing CO₂ is fundamental to the biochemistry of photosynthesis, this mechanism is recorded globally (Keeling et al., 2017). Our previous growth chamber experiments, in combination with meta-analyses, established that the effect of CO₂ on δ¹³C_p value is consistent across a wide range of species and environments (Schubert and Jahren, 2012, 2018). Recent works have also shown that the influence of CO₂ on δ¹³C_p value is not affected by water availability (Lomax et al., 2019) or atmospheric O₂ levels (Porter et al., 2017), and it is recorded within multiple organic substrates (e.g., cellulose and collagen [Hare et al., 2018], hair [Zhao et al., 2019], and *n*-alkanes [Wu et al., 2017]) and inorganic substrates (e.g., speleothems [Breecker, 2017] and cave air [Bergel et al., 2017]). Consequently, researchers now correct δ¹³C values for changes in CO₂ across a myriad of fossil (e.g., ungulate teeth [Luyt et al., 2019; Sealy et al., 2019], soil-respired carbon [Caves Rugenstein and Page Chamberlain, 2018], soil carbonate [Basu et al., 2019], pyrogenic carbon and *n*-alkanes [Zhou et al., 2017], and pollen [Bell et al., 2019]), and modern (e.g., fungi [Hobbie et al., 2017] and leaves [Tibby et al., 2016]) substrates, and recent experiments have shown that the δ¹³C_p value can produce accurate estimates of paleo-CO₂ concentration (Porter et al., 2019).

METHODS

We reconstructed CO₂ across the past 23 m.y. using a compilation of 700 δ¹³C measurements gathered from 12 previously published studies of terrestrial organic matter (TOM; *n* = 441) and plant lipids (*n* = 259) that spanned at least 1 m.y. of the Neogene (Table S1 in the Supplemental Material¹). We chose these substrates

*E-mail: schubert@louisiana.edu

¹Supplemental Material. Description of the inputs used to calculate atmospheric CO₂ concentration, uncertainty in CO_{2(t)}, Figure S1, and Tables S1 and S2. Please visit <https://doi.org/10.1130/GEOL.S.12307451> to access the supplemental material, and contact editing@geosociety.org with any questions.

because both TOM and plant lipid $\delta^{13}\text{C}$ values have been shown to respond similarly to changes in CO_2 (Schubert and Jahren, 2012; Wu et al., 2017; Chapman et al., 2019); these substrates also represent an integrated signal with multiple photosynthetic inputs, which has been shown to improve the accuracy of the proxy (Porter et al., 2019). For studies that reported $\delta^{13}\text{C}_p$ data for multiple *n*-alkanes (e.g., *n*- C_{27} , *n*- C_{29} , *n*- C_{31}), we selected only one record, or the weighted mean values (if reported), thus avoiding redundancy in our compiled data set. The $\delta^{13}\text{C}_p$ data set used for input exhibited a large range in $\delta^{13}\text{C}_p$ values ($\sim 8\%$), sampled from a wide range of environments; plant lipids generally exhibited lower $\delta^{13}\text{C}_p$ values than TOM of the same age, as is commonly observed (e.g., Chikaraishi and Naraoka, 2003). We limited our literature compilation to records with $\delta^{13}\text{C}_p$ values of TOM $\leq -22.0\%$ and plant lipids $\leq -27.0\%$, thus avoiding $\delta^{13}\text{C}_p$ values that reflected C_4 ecosystems (O'Leary, 1988). Less than 2% of all compiled $\delta^{13}\text{C}_p$ values fell above these thresholds, and these were determined to be statistical outliers (all values are reported in Figure 1 and in Table S1).

The approach used here to reconstruct atmospheric CO_2 concentration based on changes in $\delta^{13}\text{C}_p$ value was first described by Schubert and Jahren (2012) and then demonstrated by Schubert and Jahren (2015). This approach calculates CO_2 based on changes in $\delta^{13}\text{C}_p$ value

(i.e., $\delta^{13}\text{C}_{\text{anomaly}}$) between two points in time, time $t = 0$ (for which CO_2 is known) and time t (for which CO_2 is not known):

$$\delta^{13}\text{C}_{\text{anomaly}} = \frac{[(A)(B)(\text{CO}_{2(t)} + C)] / [A + (B)(\text{CO}_{2(t)} + C)] - [(A)(B)(\text{CO}_{2(t=0)} + C)] / [A + (B)(\text{CO}_{2(t=0)} + C)]}{\text{CO}_{2(t)} - \text{CO}_{2(t=0)} + \epsilon} \quad (1)$$

where A, B, and C are curve-fitting parameters ($A = 28.26$, $B = 0.22$, $C = 23.9$; Schubert and Jahren, 2012, 2015; Cui and Schubert, 2016). When calculating $\delta^{13}\text{C}_{\text{anomaly}}$, it is necessary to correct for (1) changes in the $\delta^{13}\text{C}$ value of atmospheric CO_2 between time t [$\delta^{13}\text{C}_{\text{atm}(t)}$] and time $t = 0$ [$\delta^{13}\text{C}_{\text{atm}(t=0)}$], and (2) any biosynthetic fractionation when comparing across different plant tissues (e.g., TOM and lipids). Therefore, $\delta^{13}\text{C}_{\text{anomaly}}$ represents the change in $\delta^{13}\text{C}_p$ value, after correcting for changes in the $\delta^{13}\text{C}$ value of atmospheric CO_2 ($\delta^{13}\text{C}_{\text{atm}}$) and any systematic $\delta^{13}\text{C}_p$ offset between plant tissues (ϵ), such that

$$\delta^{13}\text{C}_{\text{anomaly}} = \delta^{13}\text{C}_{p(t)} - \{[\delta^{13}\text{C}_{p(t)} - (\delta^{13}\text{C}_{\text{atm}(t)} - \delta^{13}\text{C}_{\text{atm}(t=0)})] + \epsilon\} \quad (2)$$

We can then rewrite Equation 1 in order to solve for CO_2 at any time t ($\text{CO}_{2(t)}$), as a function of $\delta^{13}\text{C}_p$ and $\delta^{13}\text{C}_{\text{atm}}$:

$$\text{CO}_{2(t)} = \{[\delta^{13}\text{C}_{p(t=0)} - \{[\delta^{13}\text{C}_{p(t)} - (\delta^{13}\text{C}_{\text{atm}(t)} - \delta^{13}\text{C}_{\text{atm}(t=0)})] + \epsilon\}] \times [A^2 + AB(\text{CO}_{2(t=0)}) + 2ABC + B^2\text{C}(\text{CO}_{2(t=0)}) + B^2\text{C}^2] + A^2B(\text{CO}_{2(t=0)})\} / \{[\delta^{13}\text{C}_{p(t=0)} - \{[\delta^{13}\text{C}_{p(t)} - (\delta^{13}\text{C}_{\text{atm}(t)} - \delta^{13}\text{C}_{\text{atm}(t=0)})] + \epsilon\}] \times [-AB - B^2(\text{CO}_{2(t=0)}) - B^2\text{C}] + A^2B\} \quad (3)$$

Descriptions of the inputs are provided in the Supplemental Material.

RESULTS

Figure 1 shows a continuous record of CO_2 across the past 23 m.y. based on changes in $\delta^{13}\text{C}_p$ value (i.e., $\delta^{13}\text{C}_{\text{anomaly}}$). We calculated that the median CO_2 value was lower than that of today across the entirety of the past 23 m.y., and it likely never fell below levels experienced during Pleistocene glacial advances (~ 170 ppm; Petit et al., 1999; Kawamura et al., 2007).

Our record commences at the start of the Neogene, when CO_2 was at a local high for the entire record (~ 350 ppmv; 23.0–22.4 Ma; Fig. 1C). During the middle Miocene (i.e., 17.1–15.4 Ma), CO_2 reached a maximum and then steadily decreased to below the threshold for Northern Hemisphere glaciation (~ 280 ppmv; DeConto et al., 2008) at the end of the Miocene. The middle Pliocene (ca. 5–3 Ma) experienced CO_2 levels that might have approached early 21st century levels (~ 400 ppmv; 84th percentile). This time period corresponds with elevated global temperatures as inferred from multiple models (Haywood et al., 2013), and sea levels up to 25 m higher than today (Miller et al., 2012; Grant et al., 2019). CO_2 declined to near or just-below pre-industrial levels during the late Pliocene, while Northern Hemisphere glaciation increased (Balco and Rovey, 2010; Bailey et al., 2013). Low CO_2 continued across the Quaternary glacial-interglacial cycles (Fig. 2) until the anthropogenic disruption in carbon cycling via the widespread use of fossil fuels (Keeling et al., 2001). Our overall record of the past 23 m.y. reveals a significant linear CO_2 decline equal to an average of 5 ppmv per million years ($p < 0.0001$). This contrasts with an average increase of 5 ppmv per decade experienced across the past 270 yr that has more than offset the CO_2 decline of the past 23 m.y.

DISCUSSION

The changes in CO_2 that we have constructed are corroborated by contemporaneous changes in various Earth cycles at the sub-epoch scale. The most important change is the long-term global cooling in progress across the Neogene, as determined by Zachos et al. (2001) based on the $\delta^{18}\text{O}$ value of foraminifera, that coincides with increased reactivity of the land surface

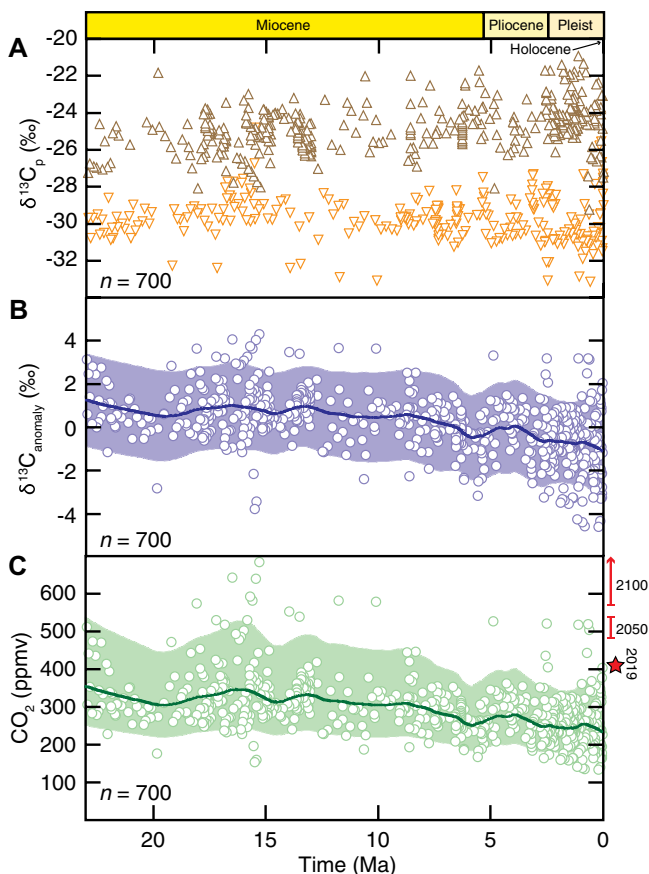


Figure 1. Reconstruction of late Cenozoic (23–0 Ma) CO_2 using C_3 plant remains. (A) Raw $\delta^{13}\text{C}_p$ values compiled from bulk terrestrial organic matter (TOM; brown; Δ) and plant lipids (orange; ∇). (B) Changes in $\delta^{13}\text{C}_p$ (i.e., $\delta^{13}\text{C}_{\text{anomaly}}$; see Equation 2). (C) CO_2 calculated using Equation 3. Present-day CO_2 (red star) and range of Intergovernmental Panel on Climate Change (IPCC) projections for the years 2050 and 2100 CE are shown for reference. Data in B and C are presented with locally weighted (LOWESS, $\alpha = 0.15$) fit through individual data points (Table S2 [see footnote 1]); shaded regions represent 84th (upper error) and 16th (low error) percentiles (see the Supplemental Material [see footnote 1]). Pleist–Pleistocene.

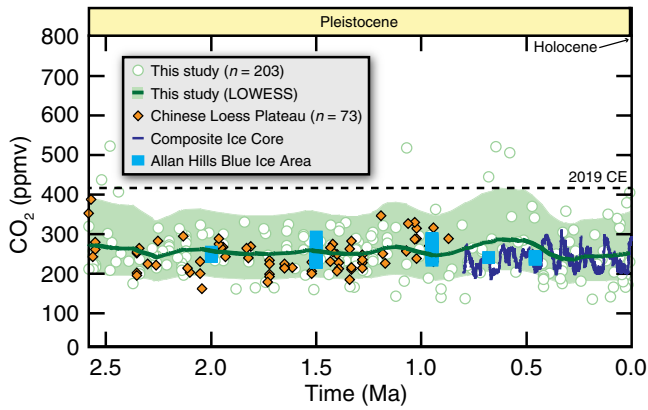


Figure 2. Reconstruction of Quaternary CO₂ using C₃ plant remains (data from Fig. 1). Paleo-soil data from the Chinese Loess Plateau (Da et al., 2019), low-resolution ice-core data (Allan Hills, Antarctica, blue ice area; Higgins et al., 2015; Yan et al., 2019), and high-resolution ice-core data (Petit et al., 1999; Monnin et al., 2001; Lüthi et al., 2008) are shown for comparison. CO₂ in 2019 CE (dashed line) is shown for reference.

(Caves Rugenstein et al., 2019), and our long-term decrease in CO₂.

In comparing our record to the sparse data available from other proxies (Fig. 3), we see that

alkenone- and stomata-based reconstructions generally estimate higher CO₂ across much of the past 23 m.y., although with overlapping uncertainties, while the δ¹¹B- and paleosol-based

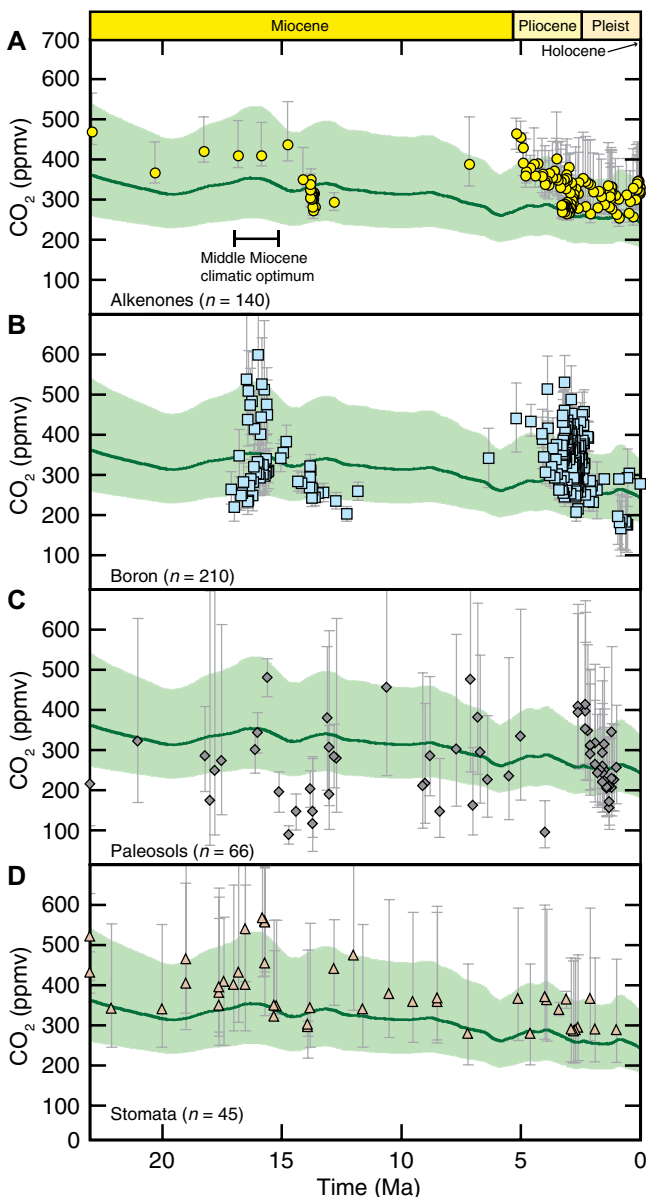


Figure 3. Late Cenozoic (23–0 Ma) CO₂ determined from (A) alkenone (Seki et al., 2010; Badger et al., 2013a, 2013b; Zhang et al., 2013), (B) boron isotope (Seki et al., 2010; Bartoli et al., 2011; Foster et al., 2012; Badger et al., 2013a; Greenop et al., 2014; Martinez-Boti et al., 2015; Stap et al., 2016), (C) paleosol (Cerling, 1992; Ekart et al., 1999; Breecker and Retallack, 2014; Da et al., 2015), and (D) stomata (Kürschner et al., 1996, 2008; Beerling et al., 2009; Grein et al., 2013; Wang et al., 2015; Reichgelt et al., 2016) proxies (as compiled within Foster et al., 2017). Our new reconstruction based on C₃ plant remains (green) is shown for reference in each panel. Note that our new record ($n = 700$; Table S2 [see footnote 1]) represents a 1.5× increase over the total number of CO₂ estimates compiled here ($n = 461$). Pleist—Pleistocene.

reconstructions do not show any consistent biases relative to our data set. In addition, the lack of continuous proxy data precludes identification of unequivocal, long-term changes in CO₂ over the past 23 m.y. (Figs. 3A–3C), except perhaps for a downward trend within the data set generated using stomatal indices (Fig. 3D).

Two key intervals of the past 23 m.y. have been cited as potential analogs for anthropogenic climate change (IPCC, 2013): the middle Miocene and Pliocene. A corresponding CO₂ increase across these two warm intervals, however, remains enigmatic (Fig. 3). For example, stomatal indices suggest CO₂ above pre-industrial levels during much of the middle Miocene (Fig. 3D), while paleosol carbonate data indicate very low CO₂ and no apparent trends (Fig. 3C). The δ¹¹B-based reconstructions do not show any clear trends during the middle Miocene, with estimates ranging from ~200 to 600 ppmv (Fig. 3B). High-resolution CO₂ data are generally lacking for the late Miocene, which makes inference of CO₂ trends during global cooling difficult to establish. In contrast, our reconstruction allows for a nearly continuous record of CO₂ that links the mid-Miocene and Pliocene warm intervals by a long-term CO₂ decline (Fig. 1C). Finally, our record reveals a CO₂ increase within the early Pliocene that is not evident when examining any single proxy, but that corresponds with mid-Pliocene warming and an inferred CO₂ increase (e.g., IPCC, 2013, their figure 5.2).

CONCLUSIONS

One of the most pressing messages that climate scientists attempt to convey to the public is that current CO₂ (2019 CE = 412 ppmv; Keeling et al., 2001) is elevated compared to the geologic past. The fact that current CO₂ is higher than it was at any time during the past ~800 k.y. is a straightforward claim based upon direct CO₂ measurements from ice cores (Petit et al., 1999; Kawamura et al., 2007) and the Mauna Loa Observatory (Keeling et al., 2001); claims associated with the more distant geologic past have been variable, partially based on a lack of consensus within the paleoclimate community. Statements addressing values from 3 m.y. ago (Willeit et al., 2019) to 15 m.y. ago (Tripathi et al., 2009) can be found, contributing to public confusion and skepticism.

Our results support the claim that CO₂ has been lower than present-day values at least across the past 7 m.y., and potentially during the entirety of the past 23 m.y.; however, CO₂ likely never fell below levels experienced during the greatest ice-sheet advances of the Pleistocene (~170 ppm; Petit et al., 1999). Our results also indirectly imply that the major reorganizations of plant (e.g., Salzman et al., 2008), animal (e.g., Stebbins, 1981), and hominid (e.g., White et al., 2009) ecosystems were not

driven by large-amplitude changes in CO₂. More meaningful, perhaps, is the inference that these reorganizations could have impelled, or been impelled by, relatively small-amplitude changes in CO₂.

Our CO₂ record differs from that gained by prior proxies in that it was produced from substrates that span 23 m.y. of uninterrupted Earth history. Our results also show good agreement with discontinuous marine and terrestrial CO₂ proxies, suggesting that the validity of the proposed mechanism underlying the effect of CO₂ on δ¹³C_p values (Schubert and Jahren, 2018) may be comparable to those of these previously confirmed CO₂ proxies. Compared to these methods, however, our proxy has the advantage of relying upon a substrate (terrestrial fossil organic carbon) that is widely available both spatially and temporally (Strauss and Peters-Kottig, 2003; Nordt et al., 2016), allowing the possibility for a near-continuous reconstruction of CO₂ across the entire evolution of C₃ land plants.

ACKNOWLEDGMENTS

We thank Peace Eze and Bryce Landreneau for assistance with data compilation. This manuscript benefited from the comments of three anonymous reviewers. This work was supported by U.S. National Science Foundation (grant EAR-1603051); the Research Council of Norway through its Centers of Excellence funding scheme (Project 223272); and the National Science Foundation of China (Grant #41888101).

REFERENCES CITED

Badger, M.P.S., Lear, C.H., Pancost, R.D., Foster, G.L., Bailey, T.R., Leng, M.J., and Abels, H.A., 2013a, CO₂ drawdown following the middle Miocene expansion of the Antarctic ice sheet: *Paleoceanography*, v. 28, p. 42–53, <https://doi.org/10.1002/palo.20015>.

Badger, M.P.S., Schmidt, D.N., Mackensen, A., and Pancost, R.D., 2013b, High-resolution alkenone palaeobarometry indicates relatively stable *p*CO₂ during the Pliocene (3.3–2.8 Ma): *Philosophical Transactions of the Royal Society: A, Mathematical, Physical and Engineering Sciences*, v. 371, p. 20130094, <http://doi.org/10.1098/rsta.2013.0094>.

Bailey, I., Hole, G.M., Foster, G.L., Wilson, P.A., Storey, C.D., Trueman, C.N., and Raymo, M.E., 2013, An alternative suggestion for the Pliocene onset of major Northern Hemisphere glaciation based on the geochemical provenance of North Atlantic Ocean ice-rafted debris: *Quaternary Science Reviews*, v. 75, p. 181–194, <https://doi.org/10.1016/j.quascirev.2013.06.004>.

Balco, G., and Rovey, C.W., II, 2010, Absolute chronology for major Pleistocene advances of the Laurentide Ice Sheet: *Geology*, v. 38, p. 795–798, <https://doi.org/10.1130/G30946.1>.

Bartoli, G., Hönisch, B., and Zeebe, R.E., 2011, Atmospheric CO₂ decline during the Pliocene intensification of Northern Hemisphere glaciations: *Paleoceanography*, v. 26, PA4213, <https://doi.org/10.1029/2010PA002055>.

Basu, S., Ghosh, S., and Sanyal, P., 2019, Spatial heterogeneity in the relationship between precipitation and carbon isotopic discrimination in C₃ plants: Inferences from a global compilation: *Global and Planetary Change*, v. 176, p. 123–131, <https://doi.org/10.1016/j.gloplacha.2019.02.002>.

Berling, D.J., Fox, A., and Anderson, C.W., 2009, Quantitative uncertainty analyses of ancient atmospheric CO₂ estimates from fossil leaves: *American Journal of Science*, v. 309, p. 775–787, <https://doi.org/10.2475/09.2009.01>.

Bell, B.A., Fletcher, W.J., Cornelissen, H.L., Campbell, J.F.E., Ryan, P., Grant, H., and Zielhofer, C., 2019, Stable carbon isotope analysis on fossil *Cedrus* pollen shows summer aridification in Morocco during the last 5000 years: *Journal of Quaternary Science*, v. 34, no. 4–5, p. 323–332, <https://doi.org/10.1002/jqs.3103>.

Bergel, S.J., Carlson, P.E., Larson, T.E., Wood, C.T., Johnson, K.R., Banner, J.L., and Breecker, D.O., 2017, Constraining the subsoil carbon source to cave-air CO₂ and speleothem calcite in central Texas: *Geochimica et Cosmochimica Acta*, v. 217, p. 112–127, <https://doi.org/10.1016/j.gca.2017.08.017>.

Breecker, D.O., 2017, Atmospheric *p*CO₂ control on speleothem stable carbon isotope compositions: *Earth and Planetary Science Letters*, v. 458, p. 58–68, <https://doi.org/10.1016/j.epsl.2016.10.042>.

Breecker, D.O., and Retallack, G.J., 2014, Refining the pedogenic carbonate atmospheric CO₂ proxy and application to Miocene CO₂: *Palaeogeography, Palaeoclimatology, Palaeoecology*, v. 406, p. 1–8, <https://doi.org/10.1016/j.palaeo.2014.04.012>.

Breecker, D.O., Sharp, Z.D., and McFadden, L.D., 2010, Atmospheric CO₂ concentration during ancient greenhouse climates were similar to those predicted for A.D. 2100: *Proceedings of the National Academy of Sciences of the United States of America*, v. 107, p. 576–580, <https://doi.org/10.1073/pnas.0902323106>.

Caves Rugenstein, J.K., and Page Chamberlain, C., 2018, The evolution of hydroclimate in Asia over the Cenozoic: A stable-isotope perspective: *Earth-Science Reviews*, v. 185, p. 1129–1156, <https://doi.org/10.1016/j.earscirev.2018.09.003>.

Caves Rugenstein, J.K., Ibarra, D.E., and von Blanckenburg, F., 2019, Neogene cooling driven by land surface reactivity rather than increased weathering fluxes: *Nature*, v. 571, p. 99–102, <https://doi.org/10.1038/s41586-019-1332-y>.

Cerling, T.E., 1992, Use of carbon isotopes in paleosols as an indicator of the P(CO₂) of the paleoatmosphere: *Global Biogeochemical Cycles*, v. 6, p. 307–314, <https://doi.org/10.1029/92GB01102>.

Chapman, T., Cui, Y., and Schubert, B., 2019, Stable carbon isotopes of fossil plant lipids support moderately high *p*CO₂ in the early Paleogene: *ACS Earth & Space Chemistry*, v. 3, p. 1966–1973, <https://doi.org/10.1021/acsearthspacechem.9b00146>.

Chikaraishi, Y., and Naraoka, H., 2003, Compound-specific δD-δ¹³C analyses of *n*-alkanes extracted from terrestrial and aquatic plants: *Phytochemistry*, v. 63, p. 361–371, [https://doi.org/10.1016/S0031-9422\(02\)00749-5](https://doi.org/10.1016/S0031-9422(02)00749-5).

Cui, Y., and Schubert, B.A., 2016, Quantifying uncertainty of past *p*CO₂ determined from changes in C₃ plant carbon isotope fractionation: *Geochimica et Cosmochimica Acta*, v. 172, p. 127–138.

Da, J., Zhang, Y.G., Wang, H., Balsam, W., and Ji, J., 2015, An early Pleistocene atmospheric CO₂ record based on pedogenic carbonate from the Chinese loess deposits: *Earth and Planetary Science Letters*, v. 426, p. 69–75, <https://doi.org/10.1016/j.epsl.2015.05.053>.

Da, J., Zhang, Y.G., Li, G., Meng, X., and Ji, J., 2019, Low CO₂ levels of the entire Pleistocene Epoch: *Nature Communications*, v. 10, p. 4342, <https://doi.org/10.1038/s41467-019-12357-5>.

DeConto, R.M., Pollard, D., Wilson, P.A., Palike, H., Lear, C.H., and Pagani, M., 2008, Thresholds

for Cenozoic bipolar glaciation: *Nature*, v. 455, p. 652–656, <https://doi.org/10.1038/nature07337>.

Ekart, D.D., Cerling, T.E., Montañez, I.P., and Tabor, N.J., 1999, A 400 million year carbon isotope record of pedogenic carbonate: Implications for paleoatmospheric carbon dioxide: *American Journal of Science*, v. 299, p. 805–827, <https://doi.org/10.2475/ajs.299.10.805>.

Foster, G.L., Lear, C.H., and Rae, J.W.B., 2012, The evolution of *p*CO₂, ice volume and climate during the middle Miocene: *Earth and Planetary Science Letters*, v. 341–344, p. 243–254, <https://doi.org/10.1016/j.epsl.2012.06.007>.

Foster, G.L., Royer, D.L., and Lunt, D.J., 2017, Future climate forcing potentially without precedent in the last 420 million years: *Nature Communications*, v. 8, p. 14845, <https://doi.org/10.1038/ncomms14845>.

Grant, G.R., Naish, T.R., Dunbar, G.B., Stocchi, P., Kominz, M.A., Kamp, P.J.J., Tapia, C.A., McKay, R.M., Levy, R.H., and Patterson, M.O., 2019, The amplitude and origin of sea-level variability during the Pliocene Epoch: *Nature*, v. 574, p. 237–241, <https://doi.org/10.1038/s41586-019-1619-z>.

Greenop, R., Foster, G.L., Wilson, P.A., and Lear, C.H., 2014, Middle Miocene climate instability associated with high-amplitude CO₂ variability: *Paleoceanography*, v. 29, p. 845–853, <https://doi.org/10.1002/2014PA002653>.

Grein, M., Oehm, C., Konrad, W., Utescher, T., Kunzmann, L., and Roth-Nebelsick, A., 2013, Atmospheric CO₂ from the late Oligocene to early Miocene based on photosynthesis data and fossil leaf characteristics: *Palaeogeography, Palaeoclimatology, Palaeoecology*, v. 374, p. 41–51, <https://doi.org/10.1016/j.palaeo.2012.12.025>.

Hare, V.J., Loftus, E., Jeffrey, A., and Ramsey, C.B., 2018, Atmospheric CO₂ effect on stable carbon isotope composition of terrestrial fossil archives: *Nature Communications*, v. 9, p. 252, <https://doi.org/10.1038/s41467-017-02691-x>.

Haywood, A.M., et al., 2013, Large-scale features of Pliocene climate: Results from the Pliocene Model Intercomparison Project: *Climate of the Past*, v. 9, p. 191–209, <https://doi.org/10.5194/cp-9-191-2013>.

Hegerl, G.C., Crowley, T.J., Hyde, W.T., and Frame, D.J., 2006, Climate sensitivity constrained by temperature reconstructions over the past seven centuries: *Nature*, v. 440, p. 1029–1032, <https://doi.org/10.1038/nature04679>.

Higgins, J.A., Kurbatov, A.V., Spaulding, N.E., Brook, E., Introne, D.S., Chimiak, L.M., Yan, Y., Mayewski, P.A., and Bender, M.L., 2015, Atmospheric composition 1 million years ago from blue ice in the Allan Hills, Antarctica: *Proceedings of the National Academy of Sciences of the United States of America*, v. 112, p. 6887–6891, <https://doi.org/10.1073/pnas.1420232112>.

Hobbie, E.A., Schubert, B.A., Craine, J.M., Linder, E., and Pringle, A., 2017, Increased C₃ productivity in Midwestern lawns since 1982 revealed by carbon isotopes in *Amanita thiersii*: *Journal of Geophysical Research: Biogeosciences*, v. 122, p. 280–288, <https://doi.org/10.1002/2016JG003579>.

Hollis, C.J., et al., 2019, The DeepMIP contribution to PMIP4: Methodologies for selection, compilation and analysis of latest Paleocene and early Eocene climate proxy data, incorporating version 0.1 of the DeepMIP database: *Geoscience Model Development, Discussion*, v. 12, p. 1–98, <https://doi.org/10.5194/gmd-12-3149-2019>.

IPCC (Intergovernmental Panel on Climate Change), 2013, *Climate Change 2013: The Physical Science Basis: Contribution of Working Group I to the Fifth Assessment Report of the Intergovernmental Panel on Climate Change*: Cambridge, UK, Cambridge University Press, 1535 p.

- Kawamura, K., Nakazawa, T., Aoki, S., Sugawara, S., Fujii, Y., and Watanabe, O., 2007, Dome Fuji ice core 338 kyr wet extraction CO₂ data, in International Geosphere-Biosphere Programme (IGBP) PAGES (Past Global Changes)/World Data Center for Paleoclimatology: Boulder Colorado, National Oceanic and Atmospheric Administration (NOAA)/National Climatic Data Center (NCDC) Paleoclimatology Program, Data Contribution Series # 2007-074 (updated August 2007).
- Keeling, C.D., Piper, S.C., Bacastow, R.B., Wahlen, M., Whorf, T.P., Heimann, M., and Meijer, H.A., 2001, Exchanges of Atmospheric CO₂ and ¹³CO₂ with the Terrestrial Biosphere and Oceans from 1978 to 2000. I: Global Aspects: San Diego, California, Scripps Institution of Oceanography (SIO), SIO Reference Series, 88 p.
- Keeling, R.F., Graven, H.D., Welp, L.R., Resplandy, L., Bi, J., Piper, S.C., Sun, Y., Bollenbacher, A., and Meijer, H.A.J., 2017, Atmospheric evidence for a global secular increase in carbon isotopic discrimination of land photosynthesis: Proceedings of the National Academy of Sciences of the United States of America, v. 114, p. 10361–10366, <https://doi.org/10.1073/pnas.1619240114>.
- Kürschner, W.M., van der Burgh, J., Visscher, H., and Dilcher, D.L., 1996, Oak leaves as biosensors of late Neogene and early Pleistocene paleoatmospheric CO₂ concentrations: Marine Micropaleontology, v. 27, p. 299–312, [https://doi.org/10.1016/0377-8398\(95\)00067-4](https://doi.org/10.1016/0377-8398(95)00067-4).
- Kürschner, W.M., Kvaček, Z., and Dilcher, D.L., 2008, The impact of Miocene atmospheric carbon dioxide fluctuations on climate and the evolution of terrestrial ecosystems: Proceedings of the National Academy of Sciences of the United States of America, v. 105, no. 2, p. 449–453, <https://doi.org/10.1073/pnas.0708588105>.
- Lomax, B.H., Lake, J.A., Leng, M.J., and Jardine, P.E., 2019, An experimental evaluation of the use of $\Delta^{13}C$ as a proxy for palaeoatmospheric CO₂: Geochimica et Cosmochimica Acta, v. 247, p. 162–174, <https://doi.org/10.1016/j.gca.2018.12.026>.
- Lüthi, D., Le Floch, M., Bereiter, B., Blunier, T., Barnola, J.-M., Siegenthaler, U., Raynaud, D., Jouzel, J., Fischer, H., Kawamura, K., and Stocker, T.F., 2008, High-resolution carbon dioxide concentration record 650,000–800,000 years before present: Nature, v. 453, p. 379–382, <https://doi.org/10.1038/nature06949>.
- Luyt, J., Hare, V.J., and Sealy, J., 2019, The relationship of ungulate $\delta^{13}C$ and environment in the temperate biome of southern Africa, and its palaeoclimatic application: Palaeogeography, Palaeoclimatology, Palaeoecology, v. 514, p. 282–291, <https://doi.org/10.1016/j.palaeo.2018.10.016>.
- Martinez-Boti, M.A., Foster, G.L., Chalk, T.B., Rohling, E.J., Sexton, P.F., Lunt, D.J., Pancost, R.D., Badger, M.P.S., and Schmidt, D.N., 2015, Plio-Pleistocene climate sensitivity evaluated using high-resolution CO₂ records: Nature, v. 518, no. 7537, p. 49–54, <https://doi.org/10.1038/nature14145>.
- Miller, K.G., Wright, J.D., Browning, J.V., Kulpecz, A., Kominz, M., Naish, T.R., Cramer, B.S., Rosenthal, Y., Peltier, W.R., and Soudian, S., 2012, High tide of the warm Pliocene: Implications of global sea level for Antarctic deglaciation: Geology, v. 40, p. 407–410, <https://doi.org/10.1130/G32869.1>.
- Monnin, E., Indermühle, A., Dällenbach, A., Flückiger, J., Stauffer, B., Stocker, T.F., Raynaud, D., and Barnola, J.-M., 2001, Atmospheric CO₂ concentrations over the last glacial termination: Science, v. 291, p. 112–114, <https://doi.org/10.1126/science.291.5501.112>.
- Nordt, L., Tubbs, J., and Dworkin, S., 2016, Stable carbon isotope record of terrestrial organic materials for the last 450 Ma yr: Earth-Science Reviews, v. 159, p. 103–117, <https://doi.org/10.1016/j.earscirev.2016.05.007>.
- O'Leary, M.H., 1988, Carbon isotopes in photosynthesis: Bioscience, v. 38, p. 328–336, <https://doi.org/10.2307/1310735>.
- Petit, J.R., et al., 1999, Climate and atmospheric history of the past 420,000 years from the Vostok ice core, Antarctica: Nature, v. 399, p. 429–436, <https://doi.org/10.1038/20859>.
- Porter, A.S., Yiotis, C., Montañez, I.P., and McElwain, J.C., 2017, Evolutionary differences in $\Delta^{13}C$ detected between spore and seed bearing plants following exposure to a range of atmospheric O₂:CO₂ ratios: Implications for paleoatmosphere reconstruction: Geochimica et Cosmochimica Acta, v. 213, p. 517–533, <https://doi.org/10.1016/j.gca.2017.07.007>.
- Porter, A.S., Evans-FitzGerald, C., Yiotis, C., Montañez, I.P., and McElwain, J.C., 2019, Testing the accuracy of new paleoatmospheric CO₂ proxies based on plant stable carbon isotopic composition and stomatal traits in a range of simulated paleoatmospheric O₂:CO₂ ratios: Geochimica et Cosmochimica Acta, v. 259, p. 69–90, <https://doi.org/10.1016/j.gca.2019.05.037>.
- Reichgelt, T., D'Andrea, W.J., and Fox, B.R.S., 2016, Abrupt plant physiological changes in southern New Zealand at the termination of the Mi-1 event reflect shifts in hydroclimate and pCO₂: Earth and Planetary Science Letters, v. 455, p. 115–124, <https://doi.org/10.1016/j.epsl.2016.09.026>.
- Royer, D.L., Donnadieu, Y., Park, J., Kowalczyk, J., and Goddard, Y., 2014, Error analysis of CO₂ and O₂ estimates from the long-term geochemical model GEOCARBSULF: American Journal of Science, v. 314, p. 1259–1283, <https://doi.org/10.2475/09.2014.01>.
- Salzmann, U., Haywood, A.M., and Lunt, D.J., 2008, The past is a guide to the future? Comparing middle Pliocene vegetation with predicted biome distributions for the twenty-first century: Philosophical Transactions of the Royal Society: A, Mathematical, Physical and Engineering Sciences, v. 367, p. 189–204.
- Schubert, B.A., and Jahren, A.H., 2012, The effect of atmospheric CO₂ concentration on carbon isotope fractionation in C₃ land plants: Geochimica et Cosmochimica Acta, v. 96, p. 29–43, <https://doi.org/10.1016/j.gca.2012.08.003>.
- Schubert, B.A., and Jahren, A.H., 2015, Global increase in plant carbon isotope fractionation following the Last Glacial Maximum caused by increase in atmospheric pCO₂: Geology, v. 43, p. 435–438, <https://doi.org/10.1130/G36467.1>.
- Schubert, B.A., and Jahren, A.H., 2018, Incorporating the effects of photorespiration into terrestrial paleoclimate reconstruction: Earth-Science Reviews, v. 177, p. 637–642, <https://doi.org/10.1016/j.earscirev.2017.12.008>.
- Sealy, J., Naidoo, N., Hare, V.J., Brunton, S., and Faith, J.T., 2019, Climate and ecology of the palaeo-Agulhas Plain from stable carbon and oxygen isotopes in bovid tooth enamel from Nelson Bay Cave, South Africa: Quaternary Science Reviews (in press), <https://doi.org/10.1016/j.quascirev.2019.105974>.
- Seki, O., Foster, G.L., Schmidt, D.N., Mackensen, A., Kawamura, K., and Pancost, R.D., 2010, Alkenone and boron-based Pliocene pCO₂ records: Earth and Planetary Science Letters, v. 292, p. 201–211, <https://doi.org/10.1016/j.epsl.2010.01.037>.
- Stap, L.B., de Boer, B., Ziegler, M., Bintanja, R., Lourens, L.J., and van de Wal, R.S.W., 2016, CO₂ over the past 5 million years: Continuous simulation and new $\delta^{11}B$ -based proxy data: Earth and Planetary Science Letters, v. 439, p. 1–10, <https://doi.org/10.1016/j.epsl.2016.01.022>.
- Stebbins, G.L., 1981, Coevolution of grasses and herbivores: Annals of the Missouri Botanical Garden, v. 68, p. 75–86, <https://doi.org/10.2307/2398811>.
- Strauss, H., and Peters-Kottig, W., 2003, The Paleozoic to Mesozoic carbon cycle revisited: The carbon isotopic composition of terrestrial organic matter: Geochemistry Geophysics Geosystems, v. 4, 1083, <https://doi.org/10.1029/2003GC000555>.
- Tibby, J., Barr, C., McInerney, F.A., Henderson, A.C.G., Leng, M.J., Greenway, M., Marshall, J.C., McGregor, G.B., Tyler, J.J., and McNeil, V., 2016, Carbon isotope discrimination in leaves of the broad-leaved paperbark tree, *Melaleuca quinque-nervia*, as a tool for quantifying past tropical and subtropical rainfall: Global Change Biology, v. 22, p. 3474–3486, <https://doi.org/10.1111/gcb.13277>.
- Tripati, A.K., Roberts, C.D., and Eagle, R.A., 2009, Coupling of CO₂ and ice sheet stability over major climate transitions of the last 20 million years: Science, v. 326, p. 1394–1397, <https://doi.org/10.1126/science.1178296>.
- Wang, Y., Momohara, A., Wang, L., Lebreton-Anberrière, J., and Zhou, Z., 2015, Evolutionary history of atmospheric CO₂ during the late Cenozoic from fossilized *Metasequoia* needles: PLoS One, v. 10, no. 7, p. e0130941, <https://doi.org/10.1371/journal.pone.0130941>.
- White, T.D., et al., 2009, Macrovertebrate paleontology and the Pliocene habitat of *Ardipithecus ramidus*: Science, v. 326, p. 67, 87–93, <https://doi.org/10.1126/science.1175822>.
- Willeit, M., Ganopolski, A., Calov, R., and Brovkin, V., 2019, Mid-Pleistocene transition in glacial cycles explained by declining CO₂ and regolith removal: Science Advances, v. 5, p. eaav7337, <https://doi.org/10.1126/sciadv.aav7337>.
- Wu, M.S., Feakins, S.J., Martin, R.E., Shenkin, A., Bentley, L.P., Blonder, B., Salinas, N., Asner, G.P., and Malhi, Y., 2017, Altitude effect on leaf wax carbon isotopic composition in humid tropical forests: Geochimica et Cosmochimica Acta, v. 206, p. 1–17, <https://doi.org/10.1016/j.gca.2017.02.022>.
- Yan, Y., Bender, M.L., Brook, E.J., Clifford, H.M., Kerneny, P.C., Kurbatov, A.V., Mackay, S., Mayewski, P.A., Ng, J., Severinghaus, J.P., and Higgins, J.A., 2019, Two-million-year-old snapshots of atmospheric gases from Antarctic ice: Nature, v. 574, p. 663–666, <https://doi.org/10.1038/s41586-019-1692-3>.
- Zachos, J., Pagani, M., Sloan, L., Thomas, E., and Billups, K., 2001, Trends, rhythms, and aberrations in global climate 65 Ma to present: Science, v. 292, no. 5517, p. 686–693, <https://doi.org/10.1126/science.1059412>.
- Zhang, Y. G., Pagani, M., Liu, Z., Bohaty, S. M., and DeConto, R., 2013, A 40-million-year history of atmospheric CO₂: Philosophical Transactions of the Royal Society: A, Mathematical, Physical and Engineering Sciences, v. 371, p. 20130096, <https://doi.org/10.1098/rsta.2013.0096>.
- Zhao, L.Z., Colman, A.S., Irvine, R.J., Karlén, S.R., Olack, G., and Hobbie, E.A., 2019, Isotope ecology detects fine-scale variation in Svalbard reindeer diet: Implications for monitoring herbivory in the changing Arctic: Polar Biology, v. 42, p. 793–805, <https://doi.org/10.1007/s00300-019-02474-8>.
- Zhou, B., Bird, M., Zheng, H., Zhang, E., Wurster, C.M., Xie, L., and Taylor, D., 2017, New sedimentary evidence reveals a unique history of C₄ biomass in continental East Asia since the early Miocene: Scientific Reports, v. 7, p. 170, <https://doi.org/10.1038/s41598-017-00285-7>.